High-speed XYZ-nanopositioner for scanning ion conductance microscopy

doi: 10.1063/1.4993296

High-speed XYZ-nanopositioner for scanning ion conductance microscopy

Shinji Watanabe, and Toshio Ando

Citation: Appl. Phys. Lett. **111**, 113106 (2017);
View online: https://doi.org/10.1063/1.4993296
View Table of Contents: http://aip.scitation.org/toc/apl/111/11
Published by the American Institute of Physics

High-speed XYZ-nanopositioner for scanning ion conductance microscopy

Shinji Watanabe[a] and Toshio Ando[b]
Bio-AFM Frontier Research Center, Institute of Science and Engineering, Kanazawa University, Kakuma-machi, Kanazawa, Ishikawa 920-1192, Japan

(Received 28 June 2017; accepted 29 August 2017; published online 15 September 2017)

We describe a tip-scan-type high-speed XYZ-nanopositioner designed for scanning ion conductance microscopy (SICM), with a special care being devoted to the way of nanopipette holding. The nanopipette probe is mounted in the center of a hollow piezoactuator, both ends of which are attached to identical diaphragm flexures, for Z-positioning. This design minimizes the generation of undesirable mechanical vibrations. Mechanical amplification is used to increase the XY-travel range of the nanopositioner. The first resonance frequencies of the nanopositioner are measured as ~100 kHz and ~2.3 kHz for the Z- and XY-displacements, respectively. The travel ranges are ~6 μm and ~34 μm for Z and XY, respectively. When this nanopositioner is used for hopping mode imaging of SICM with a ~10-nm radius tip, the vertical tip velocity can be increased to 400 nm/ms; hence, the one-pixel acquisition time can be minimized to ~1 ms. *Published by AIP Publishing.* [http://dx.doi.org/10.1063/1.4993296]

In biological research, atomic force microscopy (AFM)[1] has been widely used to visualize the topographic structure of biological specimens in physiological liquid environments.[2] Nevertheless, the cantilever tip must make contact with the sample in the solution, and even exerted forces below 10 pN considerably deform extremely soft surfaces[3,4] such as the plasma membranes of live eukaryotic cells, which prohibits high-resolution surface imaging.[5] Scanning ion conductance microscopy (SICM) is an alternative imaging method based on an entirely different working principle for capturing a topographic image[6] (Fig. 1). SICM uses an electrolyte filled glass pipette (nanopipette) as a probe and relies on an ion current flowing between an electrode inside the nanopipette and another in an external bath solution. The ion current passing through the opening of the nanopipette is sensitive to the tip-sample surface separation;[7,8] therefore, SICM can capture topographic images without any tip-sample contact.

However, the temporal resolution of SICM is much lower than that of AFM, especially when SICM is operated in the hopping mode,[9] where the tip is moved up and down to avoid lateral tip-sample contact. To achieve high resolution imaging in the hopping mode, the closest approach distance between the tip end and the sample has to be minimized to about the radius of tip opening, r_p. The time delay in the vertical tip-position control, τ_z, limits the fall velocity of the tip, v_f, namely, the speed at which the tip approaches the sample surface. Since glass nanopipettes are very fragile, they are easily damaged when they contact surfaces. To avoid surface contact, v_f must be restricted as $v_f < r_p/\tau_z$.[8] The low temporal resolution of SICM arises from the difficulty in reducing τ_z. When the bandwidth of the ion current detection is sufficiently high, the low mechanical resonance frequency of the Z-nanopositioner is the dominant contributor to the delay.[10] The difficulty in decreasing the delay is assembling the nanopipette to the Z-nanopositioner since the nanopipette is very massive and large compared to AFM cantilever tips. For instance, commercial SICM systems use a long-travel-range (~25 μm) Z-nanopositioner whose resonance frequency is less than 1 kHz when the nanopipette is assembled, producing a long delay (longer than 1 ms) for vertical tip positioning. As a result, it typically takes 10–100 ms for one-pixel acquisition when imaging samples show very rough surfaces.[9] Thus, in SICM, it is difficult to visualize morphological changes in samples which occur in less than a minute, which significantly limits the applicability of SICM in biological studies.

In this letter, we describe the design of a tip-scan-type high-speed XYZ-nanopositioner for SICM. One of the distinctive features of the developed nanopositioner is the large product of "travel range × resonance frequency" for the Z-positioner, which represents the positioner performance

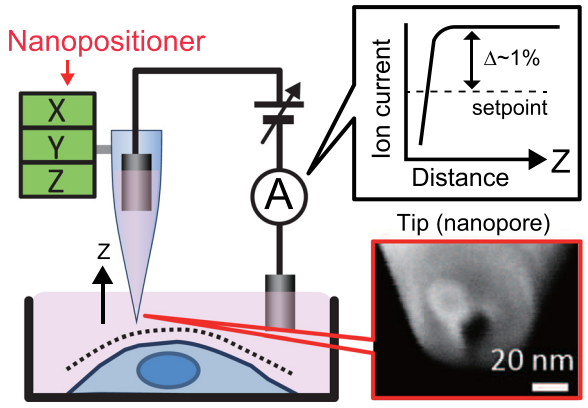

FIG. 1. Schematic of the typical SICM setup showing the working principle of SICM. The electrolyte-filled nanopipette mounted on the XYZ-nanopositioner has a nanopore at its distal end, as shown in the electron micrograph (right bottom). The ion current flowing through the nanopore induced by the application of bias voltage between two electrodes (one in the nanopipette and the other in the bath solution) is measured using the ion current detector. The ion current, which depends on the tip-surface separation as illustrated (right top), is used to control the tip Z-position during the XY-scanning of the nanopipette over the sample surface.

[a]wshinji@se.kanazawa-u.ac.jp
[b]tando@staff.kanazawa-u.ac.jp

because the travel range and resonance frequency are trade-offs. The product of our Z-positioner, 6 μm × 100 kHz, is more than ten-fold larger than those of conventional SICM systems and 2–3 times larger than that of the Z-scanner employed in high-speed AFM.[11] The performance can significantly increase v_f to 400 nm/ms and hence minimize the one-pixel acquisition time to ∼1 ms. Here, we show the detailed design and performance of our nanopositioner and demonstrate the stable high-speed imaging of test samples at 3.5 s per frame over a scan area of ∼25 × 25 μm^2 with 50 × 50 pixels.

The Z-nanopositioner mounted on the XY-nanopositioner, as illustrated in Fig. 2(a), is designed to achieve the following demands: (i) a high mechanical resonance frequency, (ii) nanopipette displacement along its length, without causing motion and vibrations in the lateral directions, and (iii) easy removal of a nanopipette from the Z-nanopositioner. The frame body of the XYZ-nanopositioner was fabricated from alloy A7075. Before constructing the actual device, we conducted a finite-element analysis (FEA) to estimate the mechanical properties of designed structures, using a commercially available finite-element package, COMSOL Multiphysics 5.0 (COMSOL AB). The following mechanical parameters for the alloy A7075/piezoactuator were used in the FEA simulation: Young's modulus, 72/33.9 GPa; Poisson's ratio, 0.3/0.3; and density, 2810/7800 kg/m^3. The central idea for suppressing unwanted mechanical vibrations in the Z-nanopositioner is the use of momentum cancellation.[12] That is, the hollow Z-piezoactuator (AE0505D08D-H0F, NEC/Tokin) is sandwiched with a pair of identical diaphragm-like flexures[13] [Fig. 2(b)] so that the center of mass of the Z-piezoactuator shows negligible changes during fast displacement. The flexures were designed to have a stiffness of ∼18.2 N/μm, which provides a suitable preload to the actuator (∼10–20 N). The magnitude of the preload is adjustable with screws.

This design can mechanically cancel dynamic forces exerted onto the Z-support frame when the Z-piezoactuator is quickly displaced. Moreover, it permits the Z-positioner to have a resonance frequency comparable to that of the Z-piezoactuator under free oscillation. Injecting epoxy glue between the diaphragm flexures and the Z-piezoactuator improved the mechanical stability of the Z-positioner and enabled its robust long-term actuation. The nanopipette is mechanically connected to the top flexure by gluing the nanopipette only to the top clamp [Fig. 2(b)] so that the nanopipette can move with the Z-movement of the top flexure. To achieve a small mass and the straight motion of the nanopipette along its length, without causing motion and vibrations in the lateral directions, first the nanopipette length was shortened from the conventional length, 35–38 mm, to ∼12–14 mm. Second, the nanopipette was laterally supported by the spacers made of an elastic material, each positioned next to one of the clamps. The spacers work as a guide for longitudinal motion of the nanopipette and avoid vibration generation in the lateral directions. To achieve easy removal of the nanopipette while ensuring its firm attachment to the clamp, the nanopipette was inserted into a polyimide tube with an inner diameter of 1 mm and a thickness of 60 μm and glued with an acrylate resin. The outer surface of the polyimide tube was also glued to the top clamp using the same resin. The polyimide tube fills the gap between the nanopipette and the clamp, allowing the use of a small amount of acrylate resin and hence the easy removal of the nanopipette; the nanopipette can be easily removed from the clamp by pushing it from the bottom. This assembly only decreases the resonance frequency of the Z-piezoactuator by 10% since the total mass of the nanopipette and clamp is much smaller than that of the Z-piezoactuator. Importantly, undesirable vibrations were suppressed in the Z-positioner below the first resonance frequency at 100 kHz. The measured first resonance frequency agreed reasonably well with the result of the FEA simulation [Fig. 3(a)]. The travel range of the Z-nanopositioner was ∼6 μm, as measured with a laser vibrometer (NLV-2500, Polytech), approximately half the original maximum displacement of the Z-piezoactuator, as expected. Since the travel range is inversely proportional to the resonance frequency,[14] the performance of our Z-nanopositioner can be evaluated from the product of travel range × resonance frequency, which at 6 μm × 100 kHz significantly exceeds (by more than 10-fold) 25 μm × 1–2 kHz in conventional SICM nanopositioners.

For XY-displacements, we used mechanical amplification[15] to magnify the original travel range (9 μm at 150 V) of XY-piezoactuators (AE0505D08DF, NEC/Tokin). In our XY-nanopositioner design, the XY-travel range can be controlled by varying the thickness of the beam flexures that connect the Z-nanopositioner and the surrounding base frame, indicated by the broken circle in Fig. 4(c), without

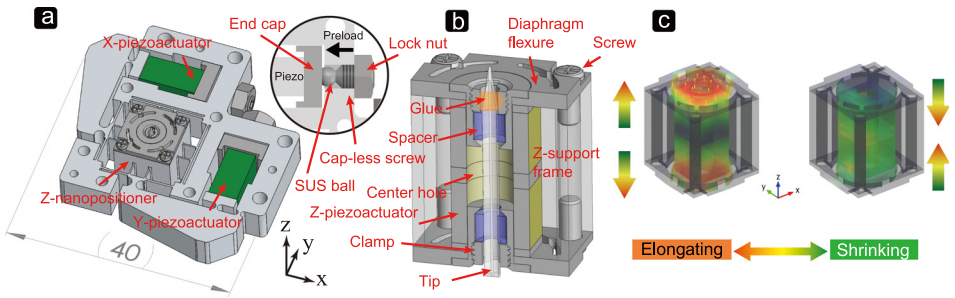

FIG. 2. (a) Drawing showing the structure of the XYZ-nanopositioner designed in this study. The base frame is 5 mm thick and 40 mm wide. The lateral scan is driven with identical piezoactuators via mechanical amplification. Preloads are applied to the X- and Y-piezoactuators using the end caps, each of which is pushed with the capless screw via a stainless steel ball. To stabilize the preload, each screw is fixed with a lock nut. (b) Cross-sectional view of the Z-nanopositioner. The glue is only applied to a contact area between the top clamp and the nanopipette. (c) Displacement of the Z-nanopositioner in the elongation (left) and shrinkage (right) actuations, as simulated by FEA. The arrows represent the vectors of local displacement from its original position.

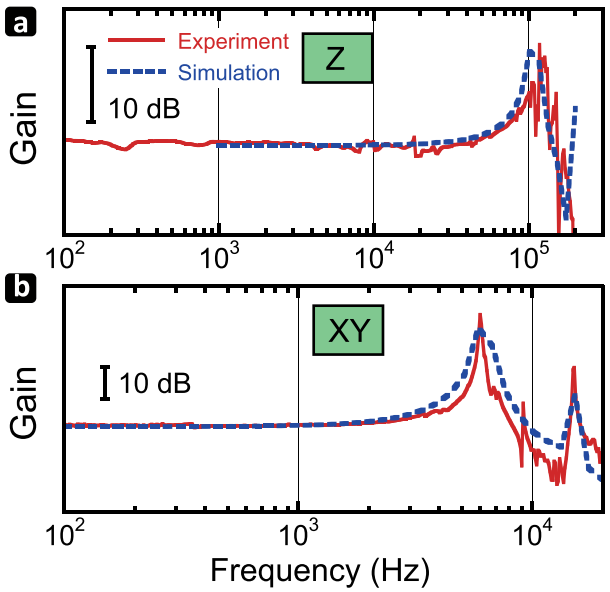

FIG. 3. Transfer function of the nanopositioner for (a) vertical and (b) lateral displacements (the phase is not shown). The solid and broken lines indicate the results from experiments and FEA simulations, respectively. The transfer functions were obtained for the 300-μm-thick beam flexures. The resonance frequency for the lateral displacement decreases from ~6 to 4.5 kHz when the full components of the Z-positioner are assembled with the XY-positioner.

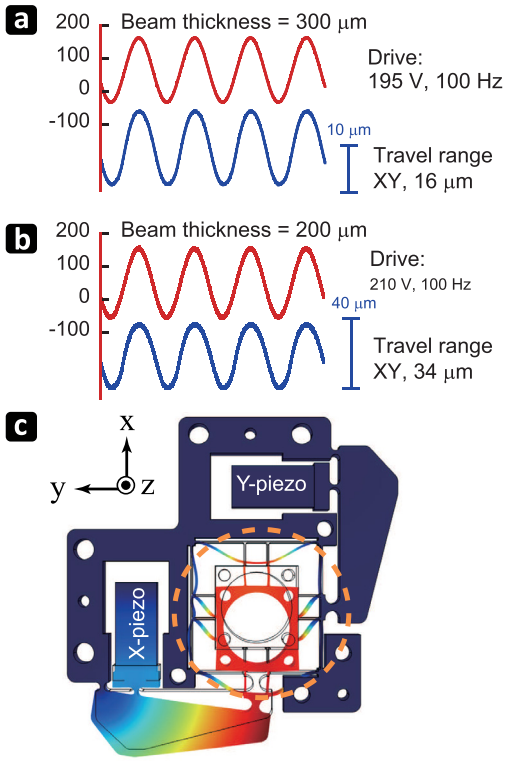

FIG. 4. Lateral displacements of the nanopositioner under 100-Hz sinusoidal voltage application. The beam flexures are (a) 300 and (b) 200 μm thick. (c) FEA simulation result for the elongation of the X-piezoactuator. In this simulation, the positions of the backside of the piezoactuator and the screw holes in the scanner frame were fixed.

changing the overall dimensions of the nanopositioner. The measured travel range increased from 16 [Fig. 4(a)] to 34 μm [Fig. 4(b)] with decreasing the beam-flexure thickness from 300 to 200 μm, which is the practical limit for fabrication by wire electrical discharge machining. The mechanical amplification factors, 1.4 and 2.7, were consistent with the results of the FEA simulation (not shown). The measured dominant resonance frequency of the XY-nanopositioner assembled with the full components of the Z-nanopositioner decreased from 4.5 to 2.3 kHz, adequate for achieving high-speed SICM, with the decreasing beam-flexure thickness (not shown).

We tested the XYZ positioner with a beam flexure with a thickness of 200 μm by imaging grating samples fabricated using polydimethylsiloxane, which had periodic 5×5 μm^2 checkerboard grid patterns with 100-nm height steps (Grating 1). To have rougher structures on the grid patterns, Scotch tape was put on the fabricated grating, left for a long time, and then removed (we refer to the resulting sample as Grating 2). The nanopipette tips were fabricated by pulling heated quartz capillaries (Q100-30-15, Sutter Instruments; outer diameter: 1.0 mm and inner diameter: 0.30 mm) using the P-2000 laser puller (Sutter Instruments). The nanopipette tip used in this study had a pore radius of ~10 nm, which was estimated by scanning electron microscopy (ZEISS) imaging and electrical resistance measurements.[16] The laboratory-built SICM instrument was controlled using a FPGA-based system (NI-5782 for Z-control, NI-5781 for XY-control with NI PXI-7954R; National Instruments) and a software program made using Labview 2015 (National Instruments). The program was also used for data acquisition and analysis. The nanopositioner was driven by piezodrivers (M-2141 for Z-positioning, MESTEK; M-26110-2-K for XY-positioning, MESTEK).

We first captured hopping-mode SICM images of Grating 1 samples immersed in a solution containing 0.15 M KCl, using a nanopipette with a pore radius of $r_p \sim 10$ nm. The v_f value and hopping amplitude were set at 400 nm/ms and 300 nm, respectively. Figure 5(a) shows a topographic image captured at 3.5 s/frame for a scan area of $\sim 25 \times 25$ μm^2 with 50×50 pixels. The image shows a grating pitch with variations of 20% in the X- and Y-directions, mainly due to the hysteresis effect of the XY-piezoactuators and partially due to the cross-coupling between them. Since it is possible to compensate for these effects by exploiting previously reported methods,[10,17] we do not focus on this issue in this study. In Fig. 5(a), no notable undesirable vibrations appeared even in the left edge region of the image, where the scanning direction was inverted, and hence, the X-positioner was driven at high frequencies. The v_f value, 400 nm/ms, used in this imaging is significantly larger than the typical v_f values used in conventional SICM systems (~20 nm/ms). Although the comparable v_f value of ~500 nm/ms was reported for a fast Z-positioner equipped with a nanopipette of $r_p \simeq 50$ nm,[8] the attainable v_f depends on r_p, as mentioned above. Therefore, our Z-positioner improved the Z-positioning latency by a factor of ~4, compared to the previously reported one.[8]

To further evaluate the performance of our XYZ-nanopositioner, we captured a topographic image of Grating 2 with rougher surfaces than Grating 1, in which wire-like objects were seen on the surface, as shown in Fig. 5(b). This image was captured at ~26 s/frame for a scan area of $\sim 25 \times 25$ μm^2 with 100×100 pixels, using a hopping amplitude of 600 nm and a v_f value of 400 nm/ms. By increasing the hopping amplitude to 600 nm, wire-like objects likely to be partially suspended between grids [Fig. 5(c)] were

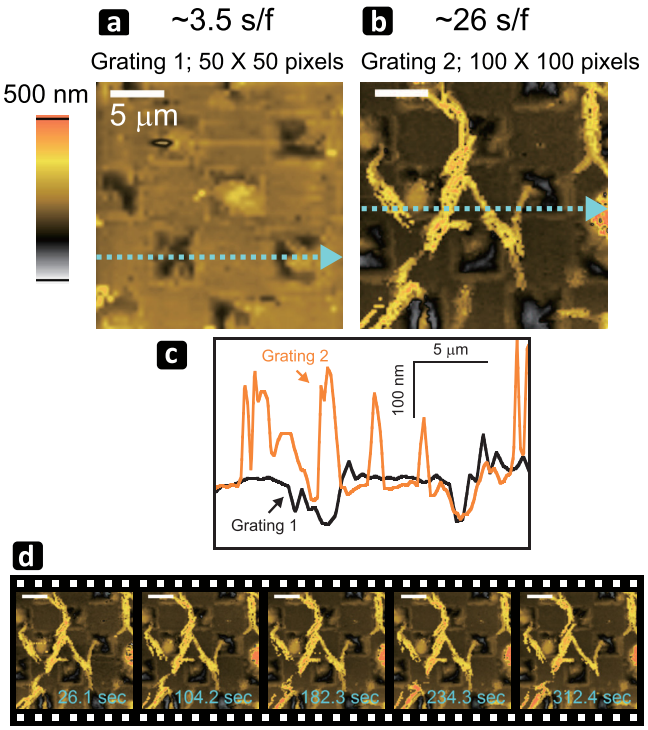

FIG. 5. SICM images of Gratings (a) 1 and (b) 2 captured at 3.5 and 26 s/frame, respectively. (c) Height profiles of images (a) and (b) along the light blue broken lines shown in (a) and (b). (d) Five images of Grating 2 clipped from successive images captured at ~26 s/frame for longer than 5 min. Scale bars, 5 μm.

captured without any signature of tip-sample contact (i.e., "tail-like patterns"[18]) although the time required for one-pixel acquisition increased from ~750 to 1500 μs. Figure 5(d) shows successive images of Grating 2 captured for longer than 5 min. These images showing no tip-sample contact are identical to each other, demonstrating the robustness of our XYZ-positioner.

In summary, we developed a tip-scan-type high-speed XYZ-nanopositioner for SICM. The installation of the nanopipette mount in the center of a hollow piezoactuator, the use of a momentum cancellation mechanism for the Z-positioner, and the nanopipette holding mechanism resulted in a high resonance frequency of 100 kHz even with a relatively long travel range (6 μm). The improved time delay of the Z-nanopositioner increases the v_f value by more than 20 times that of conventional SICM nanopositioners. These excellent features allowed the high-speed imaging of Grating 1 at 3.5 s/frame for a scan area of 25×25 μm^2 with 50×50 pixels without generating undesirable vibrations. Moreover, a rougher surface could be captured without decreasing v_f. This study is the first step toward achieving high-speed SICM that can capture biological samples in dynamic action in real time.

This work was supported by the Grant for "JST-SENTAN" (to S.W.) and the Grant for Young Scientists from Hokuriku Bank (to S.W.) and JSPS KAKENHI [Grant Nos. JP26790048 (to S.W.), JP16H00799 (to S.W.), JP24227005 (to T.A.), and JP17H06121 (to T.A.)].

[1]G. Binnig, C. F. Quate, and C. Gerber, Phys. Rev. Lett. **56**, 930 (1986).
[2]Y. F. Dufrêne, T. Ando, R. Garcia, D. Alsteens, D. Martinez-Martin, A. Engel, C. Gerber, and D. J. Müller, Nat. Nanotechnol. **12**, 295 (2017).
[3]Y. Zhou, C.-C. Chen, A. E. Weber, L. Zhou, L. A. Baker, and J. Hou, Tissue Barriers **1**, e25585 (2013).
[4]T. Ushiki, M. Nakajima, M. Choi, S.-J. Cho, and F. Iwata, Micron **43**, 1390 (2012).
[5]J. Seifert, J. Rheinlaender, P. Novak, Y. E. Korchev, and T. E. Schaffer, Langmuir **31**, 6807 (2015).
[6]P. Hansma, B. Drake, O. Marti, S. Gould, and C. Prater, Science **243**, 641 (1989).
[7]Y. E. Korchev, C. L. Bashford, M. Milovanovic, I. Vodyanoy, and M. J. Lab, Biophys. J. **73**, 653 (1997).
[8]P. Novak, A. Shevchuk, P. Ruenraroengsak, M. Miragoli, A. J. Thorley, D. Klenerman, M. J. Lab, T. D. Tetley, J. Gorelik, and Y. E. Korchev, Nano Lett. **14**, 1202 (2014).
[9]P. Novak, C. Li, A. I. Shevchuk, R. Stepanyan, M. Caldwell, S. Hughes, T. G. Smart, J. Gorelik, V. P. Ostanin, M. J. Lab, G. W. J. Moss, G. I. Frolenkov, D. Klenerman, and Y. E. Korchev, Nat. Methods **6**, 279 (2009).
[10]Y. K. Yong, K. Liu, and S. R. Moheimani, IEEE Trans. Control Syst. Technol. **18**, 1172 (2010).
[11]T. Ando, T. Uchihashi, and T. Fukuma, Prog. Surf. Sci. **83**, 337 (2008).
[12]T. Ando, N. Kodera, E. Takai, D. Maruyama, K. Saito, and A. Toda, Proc. Natl. Acad. Sci. **98**, 12468 (2001).
[13]Y. Yong and S. R. Mohemani, IEEE Trans. Nanotechnol. **12**, 137 (2013).
[14]Y. Yong, S. R. Moheimani, B. J. Kenton, and K. Leang, Rev. Sci. Instrum. **83**, 121101 (2012).
[15]Y. K. Yong, S. S. Aphale, and S. R. Moheimani, IEEE Trans. Nanotechnol. **8**, 46 (2009).
[16]Y. Fu, H. Tokuhisa, and L. A. Baker, Chem. Commun. **2009**, 4877.
[17]H. Watanabe, T. Uchihashi, T. Kobashi, M. Shibata, J. Nishiyama, R. Yasuda, and T. Ando, Rev. Sci. Instrum. **84**, 053702 (2013).
[18]D. Klenerman, Y. E. Korchev, and S. J. Davis, Curr. Opin. Chem. Biol. **15**, 696 (2011).